European Journal of Clinical Pharmacy
Print ISSN: 2385-409X **Online ISSN**: 3105-0409
Website: https://farmclin.com/

Original Research Article

Potential Therapeutic Role of Fluvoxamine in Cuprizone-Induced Demyelination Model in the Hippocampus of Adult Male Mice: A Histological and Immunohistochemical Study

Article History:

Received: 06-01-2026
Revised: 10-02-2026
Accepted: 24-02-2026
Published: 05-03-2026

Name of Author:
Nora M. Hamada [1], Mona FM Soliman [1,2], Amal Mohamed Moustafa [1], Shireen A. Mazroa [1]

Affiliation: *[1]Department of Medical Histology and Cell Biology, Faculty of Medicine, Mansoura University, Mansoura, Egypt;*
[2]Department of Medical Histology and Cell Biology, Faculty of Medicine, Horus University, New Damietta, Egypt

Corresponding Author:
Nora M. Hamada

Abstract: Demyelinating diseases are a group of disorders where the protective myelin sheath around nerve fibers is damaged, leading to disrupted neural conduction and neurological deficits. This study was performed to study the possible neuro-regenerative role of fluvoxamine (FLV) against cuprizone (CPZ) induced demyelination model in the hippocampus. Twenty-four adult male mice were divided into 3 groups. Control group I, CPZ-administered group II (0.2% orally in the diet for 8 weeks) and CPZ and FLV group III received CPZ as in group II, with oral FLV (100 mg/kg BW/day) on week 4 till the end of the experiment. After 8 weeks, the hippocampus was prepared for light and electron microscopy as well as PCNA immunohistochemical staining. Group II showed degenerative changes in hippocampus proprius (HP) and dentate gyrus (DG), including neuropil vacuolation, extensive axonal fragmentation, degeneration of pyramidal and granular neurons, splitting and focal loss of myelin sheath. PCNA immune expression was significantly decreased. In group III, there were less degenerative changes than those observed in group II, preservation of the myelin and nerve axons, and a significant increase in PCNA immune reaction. In conclusion, FLV exerts a neuro-regenerative effect against CPZ-induced demyelination model in the hippocampus of adult male mice.

Keywords: Cuprizone, fluvoxamine, hippocampus, demyelination, PCNA.

INTRODUCTION

In the past two decades, there has been a considerable increase of our knowledge regarding the pathophysiology and management of various demyelinating disorders of the nervous system. Demyelinating diseases are characterized by loss or damage of myelin sheath that surrounds nerve fibers in the central or peripheral nervous system. Myelin is essential for fast and efficient transmission of electrical impulses, so its disruption leads to slowed or blocked nerve signaling. Conditions such as multiple sclerosis, neuromyelitis optica and acute disseminated encephalomyelitis are common examples, each involving immune-mediated attacks on myelin [1, 2]. The global prevalence of such diseases is steadily increasing to 2.9 million in 2023 [3].

Experimental models are essential for understanding disease, uncovering cellular regeneration and testing new therapies, bridging the gap between basic biology and clinical treatment for complex conditions like demyelination. Cuprizone-induced demyelination

model has been widely used for this purpose because it produces reproducible, region-specific demyelination in the hippocampus and allows clear separation of demyelination and remyelination phases [4, 5].

The hippocampus is a complex brain structure embedded deep into temporal lobe. It forms an important part of the limbic system [6]. The hippocampus plays a crucial role in the processes of learning, memory formation and spatial navigation [7]. The hippocampus contains various populations of myelinated axons. Myelination of the nervous system is essential for facilitating rapid nerve conduction and providing trophic support for axons [8]. Hippocampus is also connected to cortical and subcortical regions and the extent of myelination in this region plays a role in cognitive functions and diseases [9]. Unfortunately, it is well known that in demyelinating diseases with hippocampal demyelination and memory impairment are common [10]. However, it surprising that there are only few studies focusing on myelin repair in this region.

Beyond classic immunomodulatory strategies, there is growing interest in centrally acting drugs with potential neurotrophic properties to promote myelin preservation and repair. Selective serotonin reuptake inhibitors (SSRIs) have been reported in multiple preclinical studies to modulate neuroinflammation and to enhance adult neurogenesis and neural progenitor proliferation, effects that may support tissue repair after injury [11, 12].

Fluvoxamine, an SSRI, is a well-known antidepressant drug. It is considered as first line pharmacological treatment of moderate to severe depressive disorders. In obsessive compulsive disorder, fluvoxamine has shown substantial efficacy in reducing the symptoms severity [13]. However, studies suggesting fluvoxamine as a possible treatment for demyelinating disorders are deficient [14].

Therefore, the present study aimed to evaluate the effect of fluvoxamine administration on the hippocampus of adult male mice in CPZ model of demyelination through light and electron microscopic study.

Materials and methods

Chemicals

Cuprizone [Bis (cyclohexanone) oxaldihydrazone], in the form of powder 25 grams, was purchased from Sigma Aldrich company (St. Louis, Missouri, USA). Fluvoxamine (Faverin ®), in the form of tablets 100 mg each, was purchased from Mylan Laboratories (France).

Place of the study

The current experimental study was carried out at Urology and Nephrology Center, Mansoura University and was performed in accordance with international guidelines for the care and use of laboratory animals. Approval of the Mansoura University Institution Research Board was obtained **(MD.21.05.468.R1).**

Animal groups and experimental protocol

Twenty-four adult male mice (aged 8 weeks and weighing approximately 20-25 grams) were used in the study. They were housed in a room temperature of (22 ± 2) °C at 50% ± 10% relative humidity, 12 h light/dark cycle, with free access to food pellets and water. The mice were randomly divided into three groups. **Group I (control group)** included 8 mice that were fed a standard diet and were kept without any treatment all over the experimental period. **Group II (CPZ administered group)** included 8 mice that received cuprizone for 8 weeks for induction of demyelination in a daily dose of 0.2% orally in the diet [15]. **Group III (CPZ and FLV treated group)** included 8 mice that received cuprizone for induction of demyelination as in group II (0.2% daily orally in the diet) for 8 weeks. In addition, fluvoxamine oral administration (100 mg/kg BW/day) was started on week 4 (when demyelination is expected according to Avşar, ERDEM [16]) and continued till the end of the experiment. Mice of all groups were sacrificed after 8 weeks of the experiment.

Obtaining the specimens

At the end of the experiment, the mice were anesthetized with sodium pentobarbital 50 mg/kg intraperitoneally [17]. The animals were perfused through the left ventricle with 500 ml. of 10% neutral buffered formalin. The whole brain was obtained and cut in coronal direction to expose the hippocampus. The left hippocampus was used for light microscopic and immunohistochemical studies and was oriented to be sectioned in coronal direction. The right hippocampus was used for electron microscopic study and small pieces about 1 mm3 were cut in sagittal plane direction to study the myelin in the cross section of nerve fibers.

Light microscopic study

Samples from the hippocampus were fixed in 10% neutral buffered formalin and paraffin blocks were prepared. Serial sections (5µm thickness) were cut and then stained with hematoxylin and eosin (H & E) stain [18] for identification of the histological structure of the hippocampus and silver stain (Modified Bielschowsky method) [19] for staining of the nerve fibers axons.

Immunohistochemical study

For immunohistochemical study, staining was performed with anti-PCNA for detection of cell proliferation [20]. The primary antibody for PCNA

was a mouse monoclonal antibody (anti-PCNA, clone PC10), class IgG2a. Anti-PCNA (catalogue number: MAB424, Sigma-Aldrich, St. Louis, Missouri, USA) with a dilution of 1:200 (according to manufactural company). Serial paraffin sections were deparaffinized and rehydrated and stained according to Muniz Partida and Walters [21] and Nour, Sarhan [22]. Positive control slides for PCNA were prepared from rat testis (according to the data sheet of the manufacturer company), and the positive reaction was in the form of brown nuclear reaction. Negative control slides were prepared by the same steps of immune staining after omitting the step of incubation with the primary antibody [23].

Electron microscopic study

Small specimens (1mm3) from the hippocampus were fixed in 2.5% glutaraldehyde and 2% paraformaldehyde in a 0.1 M phosphate buffer (pH 7.4) overnight. Then, specimens prepared and stained according to Woods and Stirling [24]. The specimens were examined for myelin in cross section of nerve fibers by JEOL-JEM-100 SX transmission electron microscope in the Electron Microscopy unit, Faculty of Science, Alexandria University, Egypt.

Morphometric study

Six non-overlapping fields from all animals in each group were randomly chosen for the examination and were photographed using a ToupCam digital camera (XCAM1080PHA; 2.8 pixels, UK) attached to an Olympus® microscope with 0.5 X photo adaptor (CX23LEDRF; Japan), using objective lens depending on the required analysis. The resulted images were analyzed on Intel® Core I3® based computer using Video Test Morphology® software (Russia) with a specific built-in routine for calibrated distance measurement, area measurement, automated object analysis and color intensity. It was used to assess the number of PCNA positively stained cells/field (X1000).

Statistical analysis

The morphometric data was tabulated, coded, and then analyzed using the computer program SPSS (Statistical package for social science) version 26. Descriptive statistics were calculated in the form of mean ± Standard deviation (±SD). In the statistical comparison between the different groups, the significance of difference was tested using ANOVA (One-Way Analysis of Variance) to compare between more than two groups of numerical (parametric) data followed by post-hoc Tukey for multiple comparisons. P value < 0.05 was considered statistically significant.

Results

Light microscopic results

Regarding mice mortality, one mouse in group II and one mouse in group III died during the experiment.

Hematoxylin and Eosin stain

The hippocampus of control group I was formed of two regions, the hippocampus proprius (HP) and the dentate gyrus (DG). The HP was separated from DG by the hippocampal sulcus. The HP was differentiated into CA1, CA2, CA3 & CA4 subregions. The DG surrounded CA4 by its upper & lower blades **(Figure 1a)**.

The CA1, CA2, CA3 and CA4 subregions in hippocampus proprius were similar in structure and were differentiated into the following layers from outside inside: the alveus, stratum oriens, stratum pyramidale, stratum radiatum and stratum lacunosum-moleculare. The alveus was the outermost layer and contained thick myelinated nerve fibers running horizontally, with neuroglia cells as astrocytes with large pale nuclei and oligodendroglia with darker smaller nuclei distributed among the nerve fibers. Stratum oriens showed neuroglial cells in between the thick myelinated and thin unmyelinated nerve fibers. Stratum pyramidale consisted of large densely packed pyramidal neurons, with rounded vesicular nuclei and prominent nucleoli. Stratum radiatum showed a radial streaking pattern of the nerve fibers of the apical dendrites of pyramidal neurons. Stratum lacunosum-moleculare showed thin unmyelinated horizontal nerve fibers and different neuroglial cells **(Figures 1b, 1c, 1d)**. The DG appeared differentiated into molecular, granular and polymorphic layers. The molecular layer contained thin unmyelinated nerve fibers and neuroglial cells. The granular cell layer contained compactly arranged small granular cells with vesicular nuclei and prominent nucleoli. The polymorphic layer showed scattered polymorphic nuclei of neuroglial cells among thin unmyelinated mossy fibers. The subgranular zone was seen between the granular cell layer and the polymorphic layer of the DG. It contained few characteristic spindle-shaped cells with darkly stained nuclei, different from neuroglial cells **(Figures 1e, 1f)**.

In CPZ-administered group II, degenerative changes were mostly seen in CA1, CA2, CA3 subregions of HP and DG. The neuropil appeared markedly vacuolated, and oligodendroglia were few, degenerated and showed condensed nuclei in almost all layers of HP. There was disrupted cell organization and a marked reduction in the thickness of the pyramidal cell layer. Most of pyramidal cells showed darkly stained cytoplasm and condensed nuclei with empty areas of lost pyramidal cells. Microglia cells with small dense nuclei were frequently seen among degenerated pyramidal cells **(Figures 2a, 2b)**. The DG also showed marked vacuolations of neuropil. Most of granular cells were shrunken with darkly stained

cytoplasm and condensed nuclei. The characteristic spindle-shaped cells in subgranular zone were hardly identified **(Figures 2c, 2d)**.

In CPZ and FLV treated group III, there were less degenerative changes than those observed in group II. Neuropil showed mild vacuolations. Most of oligodendroglia were more or less similar to the control group. Stratum pyramidale revealed apparent mild decrease in thickness and contained some pyramidal cells with vesicular nuclei, while others were shrunken with darkly stained cytoplasm and condensed nuclei. Areas of glial tissue were seen replacing the degenerated pyramidal cells **(Figures 2e, 2f)**. The DG also showed mild vacuolations of neuropil. The granular cell layer was widely separated from surrounding neuropil. Some granular cells were shrunken with darkly stained cytoplasm and condensed nuclei and others showed vesicular nuclei. Some characteristic spindle-shaped cells with darkly stained nuclei were seen in subgranular zone. **(Figures 2g, 2h)**.

Bielschowsky Silver stain

In control group I, the axons of nerve fibers were stained dark brown to black against pale background. They appeared continuous in almost all layers, mainly in the alveus where they were thick, closely packed and arranged horizontally parallel to stratum pyramidale. Dark brown to black stained axons of nerve fibers were also seen in the molecular layer and among granular cells in DG **(Figures 3a, 3b, 3c)**.

CPZ-administered group II revealed that most of dark brown to black stained axons of nerve fibers were degenerated, thin, interrupted, fragmented or granular, while few axons were still thick and continuous. Degenerated nerve fivers were distributed mainly in the alveus (where they were widely separated) and to less extent in the other layers and among pyramidal cells in the hippocampus proprius and also in the molecular layer and among the granular cells in the DG **(Figures 3d, 3e, 3f)**.

CPZ and FLV treated group III showed that some dark brown to black stained axons of nerve fibers appeared thick and continuous while others were thin, interrupted and fragmented, mainly in the alveus (where they were widely separated) and to less extent in other layers and among pyramidal cells in HP and also in molecular layer and among granular cells in the DG **(Figures 3g, 3h, 3i)**.

Immunohistochemical results

Immunohistochemical staining for proliferating cell nuclear antigen (PCNA)

Positive control slides for PCNA were prepared from testis and showed brown positive cytoplasmic and nuclear reaction in the spermatogonia, while negative control slides were prepared from hippocampus **(Figure 4a, 4b)**.

In control group I, a negative PCNA immune reaction was found in neurons and most of neuroglia in subregions of HP. However, a positive PCNA nuclear immune reaction was found in few nuclei of neuroglia similar to those of oligodendrocytes. Also, a positive PCNA nuclear immune reaction was found in few neurons in the granular cell layer of the DG just above the SGZ and in the characteristic spindle-shaped cells in the SGZ **(Figures 4c, 4d)**.

In CPZ-administered group II, a negative PCNA immune reaction was found in neurons and most of neuroglia in subregions of HP. However, a positive PCNA nuclear immune reaction was found in more neuroglia; few of them were similar to oligodendrocytes while most of them were similar to astrocytes distributed among degenerated neurons. Occasional neurons in the granular cell layer of the DG just above the SGZ showed positive nuclear immune reaction **(Figures 4e, 4f)**.

CPZ and FLV treated group III showed occasional neurons with positive nuclear immune reaction in the subregions of HP. A positive PCNA nuclear immune reaction was found in few nuclei of neuroglia similar to those of astrocytes and oligodendroglia. Few neurons in the granular cell layer of the DG just above the SGZ, and occasional cells in SGZ showed positive nuclear immune reaction **(Figures 4g, 4h)**.

Electron microscopic results

Ultrastructural changes of myeline surrounding nerve fibers were examined in the alveus layer of HP as it contained regularly arranged myelinated nerve fibers. In cross sections, control group I showed thick compact electron dense regularly arranged lamellar electron dense myelin sheath surrounding axons of nerve fibers containing mitochondria with intact cristae and neurofibrils **(Figure 5a)**.

CPZ-administered group II revealed that most of the nerve fibers were demyelinated or surrounded with degenerative changes in myeline sheath in the form of irregularly arranged myelin, splitting of the layers, and focal loss of the myelin. The axons of degenerated nerve fibers showed disintegration of neurofibrils and degenerated mitochondria **(Figures 5b, 5c)**.

In CPZ and FLV treated group III, some nerve fibers were myelinated with compact regular lamellar electron dense structure of myelin sheath. The axoplasm in myelinated nerve fibers contained regularly arranged neurofibrils and intact mitochondria. However, other nerve fibers showed some degenerative changes in their myelin sheath as

focal splitting of the myeline. **(Figure 5d).**

Image analysis results and statistical analysis

Number of cells (mean ± SD) with PCNA positive immune reaction in the hippocampus at a magnification x1000 in the different groups of the study

A: In Hippocampus Proprius:

Using ANOVA test: A significant (P <0.001) change was found in the mean number of the cells with PCNA positive immune reaction in hippocampus proprius among the different groups of the experiment **(Table 1 & Histogram 1)**.

Post -hoc Tukey: As compared to control group I, a high significant decrease (P=0.001) in the mean number of positive PCNA immune stained cells was noticed in group II receiving CPZ, while in group III receiving FLV with CPZ, a significant increase (P=0.034) in the mean number of positive PCNA immune stained cells was seen. Group III (CPZ+ FLV) was significantly higher when compared to group II (receiving CPZ) (P< 0.001) **(Table 1 & Histogram 1).**

B: In Dentate Gyrus:

Using ANOVA test: A significant (P <0.001) change was found in the mean number of the cells with PCNA positive immune reaction in the DG among the different groups of the experiment **(Table 1 & Histogram 1)**.

Post -hoc Tukey: As compared to control group I, there was a high significant (P < 0.001) decrease in the mean number of the cells with PCNA positive immune reaction group II (receiving CPZ), however, group III (CPZ+ FLV) showed a significant increase (P=0.048) in the mean number of the cells with PCNA positive immune reaction. Group III (CPZ+ FLV) was significantly higher when compared to group II (receiving CPZ) (P< 0.001) **(Table 1 & Histogram 1).**

RESULTS

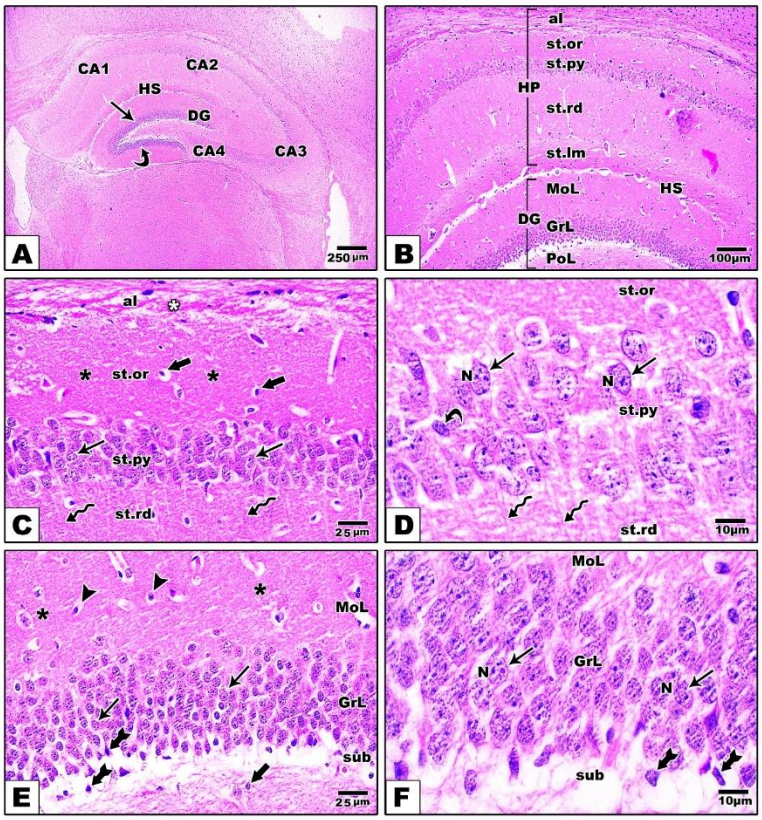

Figure 1. H&E stained sections of hippocampus in control group I **(A)** showing the different parts of the hippocampus; the hippocampus proprius differentiated into CA1, CA2, CA3 & CA4 subregions in addition to the dentate gyrus (DG) which is seen surrounding CA4 by its upper (arrow) & lower (curved arrow) blades. The hippocampus proprius is separated from the DG by the hippocampal sulcus (HS). **(B)** showing parts of CA1 and CA2 subregions in hippocampus proprius (HP) and the dentate gyrus (DG). The layers of HP from outside inside

are alveus (al), stratum oriens (st.or), stratum pyramidale (st.py), stratum radiatum (st.rd) and stratum lacunosum-moleculare (st.lm). The DG is formed of: molecular layer (MoL), the granular layer (GrL) and the polymorphic layer (PoL). Notice the presence of the hippocampal sulcus (HS) between HP and DG. **(C,D)** showing parts of the different layers in CA1 subregion; alveus (al) contains thick myelinated nerve fibers (white asterisk). Stratum oriens (st.or) has scattered neuroglial cells with small dark nuclei similar to that of oligodendrocytes (thick arrows) among the nerve fibers (black asterisks). Stratum pyramidale (st.py) consists of large densely packed pyramidal neurons (white arrows) with rounded vesicular nuclei (N) and prominent nucleoli. Note the presence of neuroglia with a large plae nucleus similar to that of astrocyte (curved arrow). Stratum radiatum (st.rd) has radially streaking pattern of the nerve fibers (zigzag arrows). **(E,F)** showing the DG differentiated into the molecular layer (MoL) containing thin unmyelinated nerve fibers (asterisks) and scattered neuroglial cells (arrow heads), granular layer (GrL) containing compactly arranged small granular cells (white arrows) with vesicular nuclei and prominent nucleoli (N), and polymorphic layer (PoL) containing scattered neuroglial cells with polymorphic nuclei (thick arrow).Note the presence of few characteristic spindle-shaped cells (tailed arrows) with darkly stained nuclei in subgranular zone (sub). **(H&E: A X 40, B X 100, C & E X 400, D & F X 1000)**

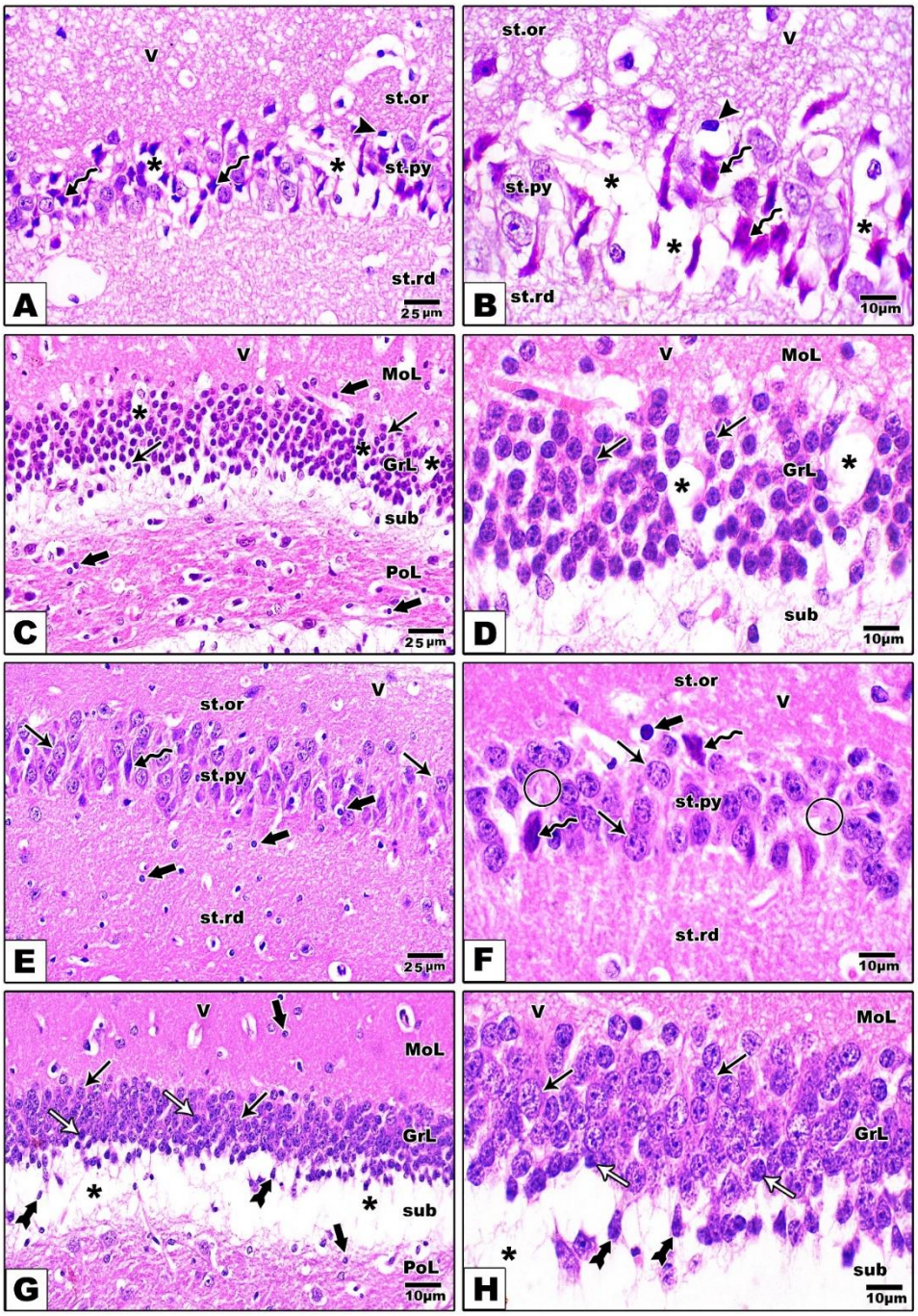

Figure 2. H&E stained sections of hippocampus in group II **(A, B, C, D)** and group III **(E, F, G, H). (A, B)** showing parts of layers in CA1 subregion; stratum oriens (st.or), stratum pyramidal (st.py) and stratum radiatum (st.rd) with markedly vacuolated neuropil (V). Stratum pyramidale reveals disrupted cell organization with marked reduction in the thickness of the pyramidal cell layer. Most of pyramidal cells show darkly stained cytoplasm and condensed nuclei (zigzag arrows). Empty areas of loss of pyramidal cells (asterisks) and microglia cells (arrow heads) with small dense nuclei are frequently seen among degenerated pyramidal cells. **(C, D)** showing the DG, the molecular layer (MoL), granular cell layer (GrL) and polymorphic layer (PoL) appear with severe vacuolations of neuropil (V). Oligodendroglia (thick arrows) appear few, degenerated with condensed nuclei. Most of granular cells are shrunken with darkly stained cytoplasm and condensed nuclei (black arrows). Empty areas of loss of granular cells (asterisks) are observed. The characteristic spindle-shaped cells (tailed arrows) in the subgranular zone (sub) are hardly identified. **(E, F)** showing parts of the different layers in CA1 subregion; stratum oriens (st.or), stratum pyramidal (st.py) and stratum radiatum (st.rd) with mild vacuolations of neuropil (V). Most of oligodendroglia (thick arrows) are more or less similar to control group. An apparent mild decrease in the thickness of pyramidal cell layer was observed. Some pyramidal cells with vesicular nuclei (white arrows) are seen, while other pyramidal cells are degenerated with darkly stained cytoplasm and condensed nuclei (zigzag arrows). Areas of glial tissue (black circles) are seen replacing the degenerated pyramidal cells. **(G, H)** showing the DG, the molecular layer (MoL), granular cell layer (GrL) and polymorphic layer (PoL) with mild vacuolations of neuropil (V). Few degenerated oligodendroglia with condensed nuclei (thick arrows) are seen. Some granular cells are shrunken with darkly stained cytoplasm and condensed nuclei (white arrows), and others show vesicular nuclei (black arrows). The granular cell layer is apparently separated from surrounding neuropil by extreme neuropil vacuolation (asterisks). Some characteristic spindle-shaped cells (tailed arrows) with darkly stained nuclei are seen in the subgranular zone (sub). **(H&E: A, C, E, G X 400, B, D, F, H X 1000)**

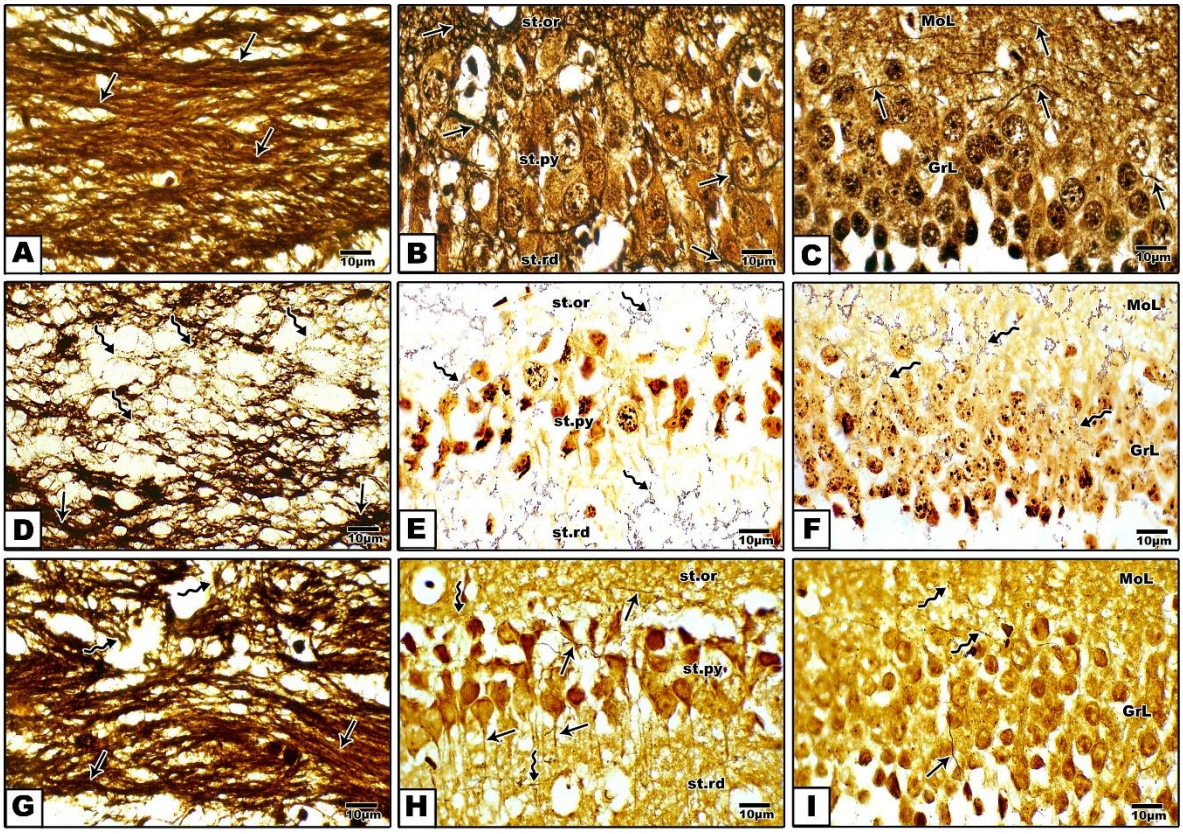

Figure 3. Silver-stained sections of hippocampus in control group I **(A, B, C)**, group II **(D, E, F)** and group III **(G, H, I)**. **(A)** showing the alveus in CA1 subregion. Dark brown to black stained axons of nerve fibers (arrows) are thick, closely packed and run in a horizontal arrangement. **(B)** CA1 subregion show continuous dark brown to black stained axons of nerve fibers (arrows) against pale background in stratum oriens (st.or), among pyramidal cells in stratum pyramidale (st.py) and in stratum radiatum (st.rd). **(C)** showing the DG with continuous, dark brown to black axons of nerve fibers (arrows) against pale background in molecular layer (MoL) and among granular cells in granular cell layer (GrL). **(D)** In the alveus, most of dark brown to black stained axons of nerve fibers are thin, widely separated,

interrupted, fragmented and granular (zigzag arrows) while few axons are still thick and continuous (arrows). **(E)** showing CA1 subregion. Most of dark brown to black stained axons of nerve fibers are thin, interrupted and fragmented (zigzag arrows) in stratum oriens (st.or), among pyramidal cells in stratum pyramidale (st.py) and in stratum radiatum (st.rd). **(F)** showing the DG, most of dark brown to black stained axons of nerve fibers are thin, interrupted, fragmented and granular (zigzag arrows). They are seen in the molecular layer (MoL) and the granular cell layer (GrL) among granular cells. **(G)** In the alveus, some brown to black stained axons of nerve fibers (arrows) are continuous and thick, while other axons are thin, widely separated, interrupted and fragmented (zigzag arrows). **(H)** showing CA1 subregion, some dark brown to black stained axons of nerve fibers appear thick and continuous (arrows) while other axons are thin, interrupted and fragmented (zigzag arrows) in stratum oriens (st.or), among pyramidal cells in stratum pyramidale (st.py) and in stratum radiatum (st.rd). **(I)** showing the molecular layer (MoL) and the granular cell layer (GrL) of DG containing some continuous dark brown to black stained axons of nerve fibers (arrow). Note the presence of some thin, interrupted axons (zigzag arrows) among granular cells. **(Silver stain: A-I X 1000)**

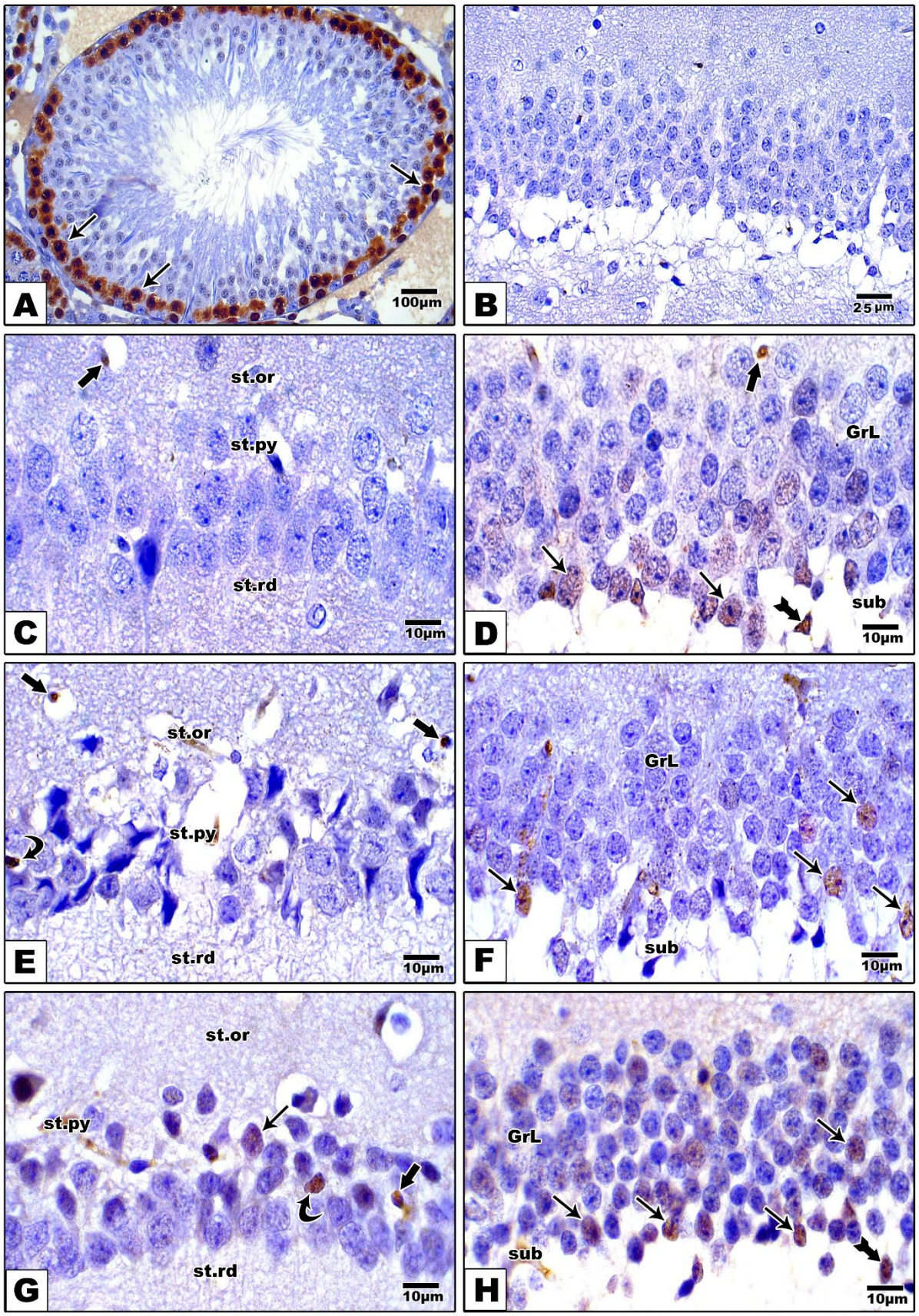

Figure 4. PCNA immuno-stained reaction. **(A,B)**: positive and negative control, **(C,D)**: control group I, **(E,F):** group II and **(G,H)**: group III. **(A):** Positive control prepared from the testis shows brown positive cytoplasmic and nuclear immune reaction for PCNA in the spermatogonia (arrows). **(B)** Negative control prepared from hippocampus after omitting the primary Ab showing absence of the immune reaction. **(C)** parts of CA1 subregion showing a negative

immune reaction in stratum oriens (st.or), stratum pyramidale (st.py) and stratum radiatum (st.rd). Note a positive immune reaction in a small nucleus of neuroglia similar to that of oligodendrocyte (thick arrow). **(D)** the DG showing a positive nuclear immune reaction in one oligodendroglial cell (thick arrow) and in few neurons (arrows) in the granular cell layer (GrL) just above the subgranular zone (sub). Note the positive immune reaction in a nucleus (tailed arrow) of the characteristic spindle-shaped cell in the subgranular zone (sub). **(E)** parts of CA1 subregion showing negative nuclear immune reaction in stratum oriens (st.or), stratum pyramidale (st.py) and stratum radiatum (st.rd). Note a positive immune reaction in a small nucleus of neuroglia similar to that of oligodendrocyte (thick arrow) and a large nucleus similar to that of astrocyte (curved arrow) among degenerated pyramidal cells. **(F)** the DG showing a positive nuclear immune reaction in occasional neurons (arrows) in the granular cell layer (GrL) just above the subgranular zone (sub). **(G)** parts of CA1 subregion showing a positive nuclear immune reaction in one neuron (arrow) and in a large nucleus similar to that of astrocyte (curved arrow) and oligodendroglial cell (thick arrow) in stratum oriens (st.or), stratum pyramidale (st.py) and stratum radiatum (st.rd) **(H)** the DG showing a positive nuclear immune reaction in few neurons (arrows) in the granular cell layer (GrL) just above the SGZ (sub) and in one cell in the SGZ (tailed arrow).

(PCNA IHC: A, B X 400, C-H X 1000)

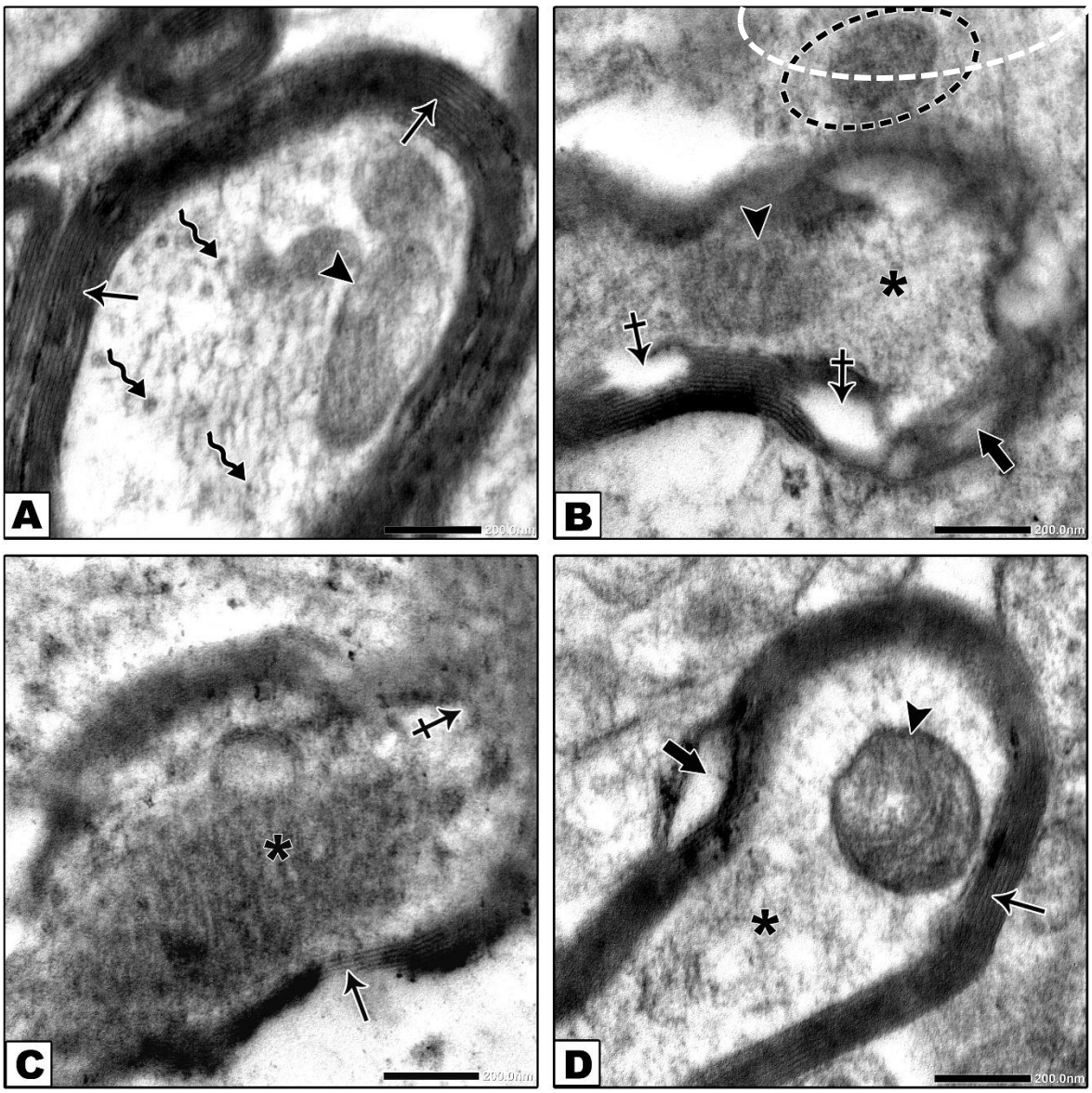

Figure 5. Electron micrographs in the alveus layer of CA1 subregion of HP. **(A)** control group I showing cross section of myelinated nerve fibers with thick compact electron dense lamellae (arrows) of myelin sheath around the axon containing mitochondria (arrow heads) and neurofibrils (zigzag arrows). **(B)** group II showing degenerated nerve

fiber with splitting of layers of myelin sheath (thick arrow) and focal loss (crossed arrows) of the myelin in some areas. Note the disintegration of neurofibrils (asterisk) and degeneraed mitochondria (arrow head) in the axon of the nerve fiber. A demylinated degenerated nerve fiver is also noted (dashed white outline). **(C)** group II showing degenerated nerve fiber surrounded with remennants of the myelin sheath (arrow) and an area of focal loss (crossed arrow) of the myelin. Note the disintegration of neurofibrils (asterisk). **(D)** group III showing a myelinated nerve fiber with compact lamellar structure of myelin sheath (arrow) around the axon containing mitochondria (arrow head) and neurofibrils (asterisks). Note the focal splitting (thick arrow) in some areas of the myelin sheath. **(TEM; A, B, C & D X 30000)**

Table (1): Number of cells (mean± SD) with positive PCNA immune reaction in different groups of the experiment.

	Group I	**Group II (CPZ)**	**Group III (CPZ and FLV treated group)**	**Test of significance (ANOVA)**
Hippocampus proprius	6.17 ± 1.83	3.25 ± 0.71 $P_{1=}$ **0.001****	8.13 ± 1.25 $P_{2=}$ **0.034***	**F = 18.457** **P < 0.001****
			P_3 **< 0.001****	
DG	9.33 ± 1.21	4.63 ± 1.06 P_1 **< 0.001****	10.88 ± 1.36 $P_{2=}$**0.048***	**F = 20.802** **P < 0.001****
			P_3 **< 0.001****	

SD: standard deviation, F for ANOVA test
* Statistically significant results if P ≤0.05
** Highly statistically significant result if P ≤0.001
P1: Significance between group II and control group I
P2: Significance between group III and control group I
P3: Significance between group III and group II

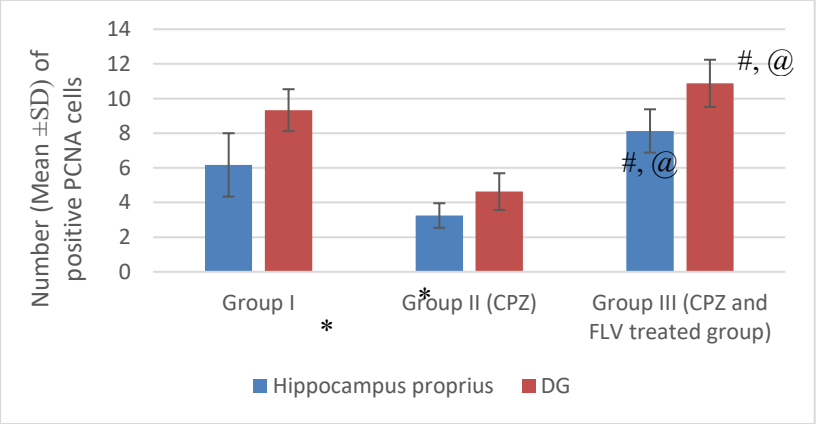

*: Significance between group II and control group I
#: Significance between group III and control group I

@: Significance between group III and group II

Histogram (1): Number (mean±SD) of cells with PCNA positive immune reaction in different groups of the experiment

DISCUSSION

The current study was done to evaluate the effect of CPZ administration as a model of demyelination on the microscopic structure of the hippocampus, and to assess the effect of fluvoxamine administration through a histological and immunohistochemical study by the light microscope, in addition to studying the electron microscopic changes in the myelin of the nerve fibers in adult male mice. Examination of H&E sections in the hippocampus of the control group I showed that the hippocampus was formed of HP and DG. The HP was differentiated into CA1, CA2, CA3 & CA4 subregions. Each subregion was further differentiated into alveus, stratum oriens, stratum pyramidale, stratum lucidum (in CA3 only), stratum radiatum and stratum lacunosum-moleculare. The DG was differentiated into molecular, granular and polymorphic layers. SGZ was seen between the granular cell layer and the polymorphic layer of the DG and contained few characteristic spindle-shaped cells different from interneurons and neuroglial cells. A similar description was provided by Treuting, Dintzis [25] and Mescher [26].

In many adult tissues, cell loss occurring through natural injury is balanced by the proliferation and differentiation of stem cells. Neurogenesis is the process by which new neurons are formed from neural stem cells (NSCs) in the brain. This process is most active during prenatal development, but it also continues in certain brain regions throughout adulthood. Adult NSCs are mainly found in the subventricular zone of the lateral ventricle and the SGZ of the hippocampal DG [27]. Neural stem cells are defined as multipotent, self-renewing cells in the CNS that are characterized by their ability to differentiate into neurons, astrocytes and oligodendrocytes. Adult NSCs have been identified as an endogenous source of neuro-regenerative cells that are mobilized during normal adult neurogenesis as well as in pathological conditions, after acute brain and spinal cord injury, stroke, epileptic seizures and intracerebral hemorrhage [28]. Adult NSCs appear with spindle or elongated cell bodies with extended processes projecting through the granule cell layer [29].

PCNA is a nuclear protein used as a marker of cell proliferation in dividing cells and sometimes for DNA repair/maintenance in non-dividing cells [30]. PCNA immune-stained section of control group I hippocampus showed a negative PCNA immune reaction in almost all the neurons and neuroglia. However, a positive PCNA nuclear immune reaction was found in few nuclei of neuroglia similar to oligodendrocytes and in the nuclei of the characteristic spindle-shaped cells in the SGZ in addition to few neurons in the granular cell layer of the DG just above the SGZ. The current results are in agreement with the data of Alonso-Moreno, Gallardo-Caballero [31].It has been reported that the cells that are PCNA positive tend to be localized in regions of adult neurogenesis, especially the SGZ of the DG [30].

The nerve fibers in the hippocampus were studied using silver stain and electron microscopy. Silver stained the axons of nerve fibers in control group I which appeared dark brown to black. They were thick, closely packed and arranged horizontally mainly in the alveus. These findings were similar to those described by Al-Neklawy [32] and Mazher and Hassan [33]. Electron microscope demonstrated the myelin sheath surrounding nerve fibers, which appeared thick, compact and formed of regularly arranged electron dense lamellae around the axons containing mitochondria and neurofibrils. These findings were similar to those described by Kirschner and Blaurock [34].

Cuprizone-induced demyelination model was performed in group II mice. The hippocampus revealed excess vacuolations of neuropil, in addition to extensive fragmentation and clumping of nerve fibers in almost all layers of regions and subregions of the hippocampus. In addition, a marked decrease in oligodendroglia was apparent. Degeneration of nerve fibers was evident also in silver stained sections where most of the axons of nerve fibers were thin, interrupted, fragmented, granular and widely separated. These findings come in agreement with Schultz, van der Meer [35], Buonvicino, Ranieri [36] and Saber [37]. Also ultrathin sections of the hippocampus of group II revealed demyelination of most of the nerve fibers. However, few nerve fibers were still myelinated but with degenerative changes in the form of irregularly arranged myelin, splitting and focal loss of the myelin sheath, with disintegration of neurofibrils and degenerated mitochondria. These findings are similar to those demonstrated by Rodrigues-Amorim, Bozzelli [38]. It has been stated that CPZ preferentially affects mature oligodendrocytes by disrupting copper-dependent mitochondrial enzymes (e.g., cytochrome c oxidase) leading to oxidative stress and cell death. The loss of oligodendrocytes causes widespread myelin sheath degradation. When myelin breaks down, it leaves behind lipid-rich debris and empty spaces in the neuropil resulting in fragmentation and clumping of

nerve fibers ([39]. Fragmentation reflects axonal breakdown and myelin disintegration resulting from oxidative stress and mitochondrial dysfunction within neurons and glial cells, in addition to inflammatory microglial activation which release reactive oxygen species (ROS) and proteases that damage axonal membranes [40]. On the other hand, clumping occurs when damaged axons and myelin debris aggregate together, forming dense irregular masses. Cytoskeleton collapses within axons, causing them to retract and bunch up [41].

The CA1 subregion was the most affected one by CPZ in group II. Das, Bastian [42] reported a rapid degeneration of CA1 activity following initiation of CPZ diet including reduction in CA1 neuronal activity and synaptic transmission. CA1 neurons and axons have exceptionally high metabolic demand and are rich in mitochondria. CPZ causes mitochondrial dysfunction and oxidative stress. Therefore, the CA1's high energy consumption makes it particularly susceptible. Jhelum, Santos-Nogueira [43] stated that CA1 subregion has greater iron accumulation than CA3 or DG. CPZ disrupts iron-copper balance resulting in enhanced free-radical generation, damaging oligodendrocytes and myelin. In addition, in CA1 subregion, oligodendrocytes are less mature and fewer in number compared with other hippocampal subregions, making them more sensitive to cuprizone toxicity [44].

In the present study, CPZ administration affected hippocampal neurons as well. There was a marked reduction in the thickness of the pyramidal cell layer and most of pyramidal cells showed darkly stained cytoplasm and condensed nuclei. Areas of glial tissue were seen replacing the degenerated pyramidal cells. Most of granular cells were shrunken with darkly stained cytoplasm and condensed nuclei, as well. These findings can be explained by the established toxicology of CPZ on oligodendrocyte which normally provide metabolic and trophic support to neurons by supplying lactate as an energy substrate and secreting neurotrophic factors such as BDNF and IGF-1. Therefore, the loss of oligodendrocytes deprives neurons of these supportive mechanisms, leading to metabolic stress and eventual neuronal degeneration. These mechanisms have been previously described in CPZ models and provide an explanation for the histological alterations observed here [45-47].

In the present study, the characteristic spindle-shaped cells in the SGZ were not detected in group II CPZ model. These findings come in agreement with Zhang, Kim [48] who reported that hippocampal neurogenesis was nearly absent in CPZ-treated mice due to inhibited NSC proliferation. It has been proved that CPZ elevates cytokine and ROS levels which suppress NSC proliferation, induce apoptosis and disrupt the balance between self-renewal and differentiation. Furthermore, inflammatory mediators can shift NSCs toward astrocytic differentiation rather than neurogenesis. Reactive astrocytes proliferate in response to CPZ-induced inflammation, release further inhibitory factors (e.g., BMPs and chemokines) and contribute to structural remodelling of the neurogenic niche, making it less liberal for neurogenesis [49].

Luo, Zhang [50] and Molinari, Byrne [51], confirmed that CPZ disrupts NSC dynamics in hippocampal SGZ that negatively affects the proliferation and viability of neural stem and progenitor cells leading to diminished neurogenesis. This can explain the results of PCNA immune reaction observed in group II in our study. There was a negative PCNA immune reaction in most of neuroglia and in neurons apart from very few neurons still showing a positive nuclear immune reaction in the granular cell layer of the DG just above the SGZ. This comes in agreement with Hahn, Kwon [52] and Hahn, Kwon [53] who stated that the absence or weak expression of PCNA suggests a reduction in proliferative activity following cuprizone exposure. However, a positive PCNA nuclear immune reaction was found in our study in some nuclei of neuroglia similar to those of oligodendrocytes and astrocytes. Oligodendrocytes were few while astrocytes were markedly increased. This can be explained by Escartin, Galea [54] and Marangon, Castro e Silva [55] who showed that a positive nuclear immune reaction for PCNA in neuroglia, including astrocytes and oligodendrocytes, is an indicator of active cellular processes, such as cell proliferation or DNA repair. Oligodendrocyte precursor cells can proliferate and differentiate into mature oligodendrocytes to repair the damaged myelin sheath. A positive PCNA reaction seen in these cells could indicate repair attempt. Astrocytes react to CPZ exposure through a process called reactive astrogliosis, which involves a change in morphology and an increase in proliferation.

Fluvoxamine is a selective serotonin reuptake inhibitor (SSRI) with high affinity for the sigma-1 receptor. Recently, it has gained attention for its potential neuroprotective and anti-inflammatory properties in neurodegenerative disorders [59]. Therefore, in the present study, fluvoxamine was given to the group III mice to investigate whether it can ameliorate degenerative changes and demyelination effect of CPZ. Examination of the hippocampus in group III showed less evident degenerative changes. The vacuolations in the neuropil was a mild, but oligodendroglia were more or less similar to control group I. Axons of nerve fibers showed mild fragmentation and clumping. Silver-stained sections of group III showed that some axons of nerve fibers appeared continuous while others were thin, interrupted and fragmented. These findings can

be explained by Bu, Liu [56] who stated that SSRI promoted proliferation and differentiation of oligodendrocyte precursor cells and restored myelin integrity in a corticosterone-induced myelin damage model.

Examination of the myelin in ultrathin sections of the hippocampus in group III revealed that some nerve fibers were myelinated with compact lamellar structure of myelin sheath around the axons, while others were demyelinated or myelinated with degenerative changes as focal splitting of the myelin sheath. These findings are similar to that of Ghareghani, Zibara [14] who stated that FLV enhances remyelination by stimulating the proliferation and differentiation of NSCs into new oligodendrocytes. In addition, FLV significantly decreased the area of demyelination plaques in the spinal cord. This was accompanied by an increase in Myelin Basic Protein (MBP) expression, a marker for myelin. Besides, FLV has been noted with anti-inflammatory effect by regulating the function of ER-resident protein sigma-1 receptor (S1R), an important modulator for innate and adaptive immune responses [57]. In addition, FLV decreased pro-inflammatory cytokines (IFN-γ) and increasing anti-inflammatory ones (IL-4). This reduced neuroinflammation creates a more favorable environment for myelin repair [58]. Experimental studies using animal models of other neurodegenerative disorders as multiple sclerosis (MS) have demonstrated that FLV can reduce demyelination, limit immune cell infiltration and attenuate disease severity. These effects are believed to arise from suppression of pro-inflammatory cytokines (such as IFN-γ and TNF-α) and upregulation of anti-inflammatory markers like IL-4. Moreover, fluvoxamine has been shown to promote neural stem cell proliferation and oligodendrocyte differentiation, enhancing remyelination through increased expression of myelin basic protein (MBP). Its activation of the sigma-1 receptor may also reduce endoplasmic reticulum stress and protect against mitochondrial dysfunction [59, 60].

Regarding the changes in the neurons in the hippocampus of group III mice of the present study, a mild decrease in the thickness of pyramidal cell layer was observed. Some pyramidal cells had vesicular nuclei while others were shrunken with darkly stained cytoplasm and condensed nuclei. Similarly, some granular cells had vesicular nuclei, while others were shrunken with darkly stained cytoplasm and condensed nuclei. The characteristic spindle-shaped cells with darkly stained nuclei were seen. These findings come in agreement with Shi, Mi [61] who showed that FLV reduces peripheral immune cell infiltration, neuronal apoptosis, BBB disruption and tissue damage after injury. Also, Tepebaşı, Aşcı [62] stated that FLV treatment was shown to increase apelin expression (an endogenous neuropeptide associated with neuroprotection, inflammation regulation and oxidative stress reduction) while reducing markers of inflammation and oxidative stress as GFAP. This proves that FLV has neuroprotective effects. In addition, Elbeltagy, Mansour [63] demonstrated that FLV has neuroprotective capability by attenuating neurotoxin-induced-dopaminergic degeneration in an animal model of Parkinson's disease. This can explain the results of the immune reaction of PCNA detected in group III of the present study. A positive PCNA immune reaction was seen in few nuclei of neuroglia similar to astrocytes and oligodendrocytes, in addition to a positive nuclear immune reaction in some neurons in the granular cell layer of DG just above the SGZ. These findings come in agreement with Ghareghani, Zibara [14] who found that FLV enhanced cell proliferation, viability and differentiation of astrocytes, oligodendrocytes and neural stem cells.

Conclusion

Cuprizone (CPZ) provided an acceptable model of demyelination as it produced structural neurodegenerative and demyelinated changes. Fluvoxamine (FLV) partially regenerated myelin and helped in neuro-regeneration in CPZ model of demyelination induced in the hippocampus of adult mice.

Disclosure statement

No potential conflict of interest was reported by the author(s).

Funding

The author(s) reported there is no funding associated with the work featured in this article.

Author contributions

Conceptualization, technique, software validation, formal analysis, resource data curation, writing, original draught preparation, writing, review, and editing Nora M. Hamada, Mona FM Soliman, Amal Mohamed Moustafa, and Shireen A. Mazroa. All authors have read and agreed to the published version of the manuscript.

Data availability statement

All data is contained within the a

References

1. Bernardo, A. and S. Visentin, Demyelinating diseases: from molecular mechanisms to therapeutic strategies. International Journal of Molecular Sciences, 2023. 24(5): p. 4596.
2. Arachchige, A.S.P.M., et al., A review of multiple sclerosis: From pathophysiology to latest therapeutic advances. AIMS Neuroscience, 2025. 12(4): p. 514-538.
3. Kapica-Topczewska, K., et al., Epidemiology of multiple sclerosis: Global

trends, regional differences, and clinical implications. Polish Journal of Neurology and Neurosurgery, 2025. 59(4): p. 375-384.
4. Kipp, M., How to use the cuprizone model to study de-and remyelination. International Journal of Molecular Sciences, 2024. 25(3): p. 1445.
5. Leo, H. and M. Kipp, Remyelination in multiple sclerosis: findings in the cuprizone model. International Journal of Molecular Sciences, 2022. 23(24): p. 16093.
6. Schirrmacher, V., Brain and Immune System Part II—An Integrative View upon Spatial Orientation, Learning, and Memory Function. International Journal of Molecular Sciences, 2025. 26(23): p. 11567.
7. Albadawi, E.A., Structural and functional changes in the hippocampus induced by environmental exposures. Neurosciences Journal, 2025. 30(1): p. 5-19.
8. Mehdipour, M., V. Thakkar, and S. Chang, Enhancing peripheral nerve regeneration in aging: the role of Schwann cells, c-Jun, and emerging therapeutic strategies. GeroScience, 2025. 47(5): p. 1-22.
9. Klein, B., et al., DCX+ neuronal progenitors contribute to new oligodendrocytes during remyelination in the hippocampus. Scientific reports, 2020. 10(1): p. 1-17.
10. Hahn, K.R., I.K. Hwang, and D.Y. Yoo, Low-Intensity Physical Exercise is Associated with Improved Myelination and Reduced Microglial Activation in a Cuprizone-Induced Demyelination Model. Neurochemical Research, 2025. 50(3): p. 182.
11. Higuchi, Y. and H. Arakawa, Serotonergic mediation of the brain-wide neurogenesis: Region-dependent and receptor-type specific roles on neurogenic cellular transformation. Current Research in Neurobiology, 2023. 5: p. 100102.
12. Izumi, Y., et al., SSRIs differentially modulate the effects of pro-inflammatory stimulation on hippocampal plasticity and memory via sigma 1 receptors and neurosteroids. Translational psychiatry, 2023. 13(1): p. 39.
13. Haddad, M., et al., The Efficacy of Fluvoxamine in Anxiety Disorders and Obsessive-Compulsive Disorder: An Overview of Systematic Reviews and Meta-Analyses. Pharmaceuticals, 2025. 18(3): p. 353.
14. Ghareghani, M., et al., Fluvoxamine stimulates oligodendrogenesis of cultured neural stem cells and attenuates inflammation and demyelination in an animal model of multiple sclerosis. Scientific reports, 2017. 7(1): p. 1-17.
15. Gingele, S., et al., Delayed demyelination and impaired remyelination in aged mice in the cuprizone model. Cells, 2020. 9(4): p. 945.
16. Avşar, T., et al., Investigation of neuro-inflammatory parameters in a cuprizone induced mouse model of multiple sclerosis. Turkish Journal of Biology, 2021. 45(5): p. 644-655.
17. Abudalo, R., et al., Mitigation of cisplatin-induced cardiotoxicity by Isorhamnetin: Mechanistic insights into oxidative stress, inflammation, and apoptosis modulation. Toxicology Reports, 2024. 12: p. 564-573.
18. Layton, C. and J.D. Bancroft, The hematoxylins and eosin, in Bancroft's Theory and Practice of Histological Techniques E-Book, K.S. Suvarna, C. Layton, and J.D. Bancroft, Editors. 2018, Elsevier Health Sciences: New York, USA. p. 126-138.
19. Highley, J.R. and N. Sullivan, Neuropathology and muscle biopsy techniques, in Bancroft's Theory and Practice of Histological Techniques E-Book, K.S. Suvarna, C. Layton, and J.D. Bancroft, Editors. 2018, Elsevier Health Sciences: New York, USA. p. 306-336.
20. Li, J., et al., Targeting PCNA/PARP1 axis inhibits the malignant progression of hepatocellular carcinoma. Frontiers in Pharmacology, 2025. 16: p. 1571786.
21. Muniz Partida, C. and E. Walters, A novel immunohistochemical protocol for paraffin embedded tissue sections using free-floating techniques. Frontiers in Neuroanatomy, 2023. 17: p. 1154568.
22. Nour, M.S., et al., Histological and immunohistochemical study of cardiac telocytes in a rat model of isoproterenol-induced myocardial infarction with a reference to the effect of grape seed extract. Acta histochemica, 2017. 119(7): p. 747-758.
23. Mazroa, S.A., Immunohistochemistry: a need for standardization. Egyptian Journal of Histology, 2012. 35(2): p. 191-197.
24. Woods, A.E. and J.W. Stirling, Transmission electron microscopy, in Bancroft's Theory and Practice of Histological Techniques, K.S. Suvarna, C. Layton, and J.D. Bancroft, Editors. 2018, Elsevier Health Sciences: New York, USA. p. 434-475.
25. Treuting, P.M., S. Dintzis, and K.S. Montine, Comparative Anatomy and Histology: A Mouse, Rat, and Human Atlas. 2017: Elsevier Science.
26. Mescher, A.L., Junqueira's Basic Histology: Text and Atlas, Seventeenth Edition. 17th edition ed. 2023, USA: McGraw Hill LLC.
27. Bagheri-Mohammadi, S.J.I.J.o.N., Adult

neurogenesis and the molecular signalling pathways in brain: the role of stem cells in adult hippocampal neurogenesis. 2022. 132(12): p. 1165-1177.
28. Bayleyegn Derso, T., et al., Neural stem cells in adult neurogenesis and their therapeutic applications in neurodegenerative disorders: a concise review. Frontiers in Molecular Medicine, 2025. 5: p. 1569717.
29. Liang, Z., N. Jin, and W. Guo, Neural stem cell heterogeneity in adult hippocampus. Cell Regeneration, 2025. 14(1): p. 6.
30. Terreros-Roncal, J., et al., Methods to study adult hippocampal neurogenesis in humans and across the phylogeny. Hippocampus, 2023. 33(4): p. 271-306.
31. Alonso-Moreno, M., et al., Human adult hippocampal neurogenesis in health and disease. Aging Brain, 2025. 8: p. 100145.
32. Al-Neklawy, A.F., Does oral chloroquine affect the hippocampus in rats? A clue to chloroquine induced neuropsychiatric adverse effects. Ain Shams Medical Journal, 2020. 71(1): p. 59-79.
33. Mazher, K.M. and R.M. Hassan, Histological, histochemical, and immunohistochemical studies of hippocampus in male New Zealand rabbits. 2021. 304(2): p. 393-399.
34. Kirschner, D.A. and A.E. Blaurock, Myelin Structure and Components, in Myelin, R.E. Martenson, Editor. 2023, CRC Press: New York, USA. p. 3-80.
35. Schultz, V., et al., Acutely damaged axons are remyelinated in multiple sclerosis and experimental models of demyelination. Glia, 2017. 65(8): p. 1350-1360.
36. Buonvicino, D., G. Ranieri, and A. Chiarugi, Cuprizone-dependent de/remyelination responses and functional correlates in mouse strains adopted to model relapsing, chronic and progressive experimental autoimmune encephalomyelitis. Neurotoxicity Research, 2021. 39(3): p. 658-666.
37. Saber, S.M., Melatonin Potentiates the Curative Effect of Mesenchymal Stem Cells in Subcortical White Matter Tissues of Cuprizone Treated Mice Model of Multiple Sclerosis. Egyptian Journal of Histology, 2024. 47(2): p. 792-802.
38. Rodrigues-Amorim, D., et al., Multisensory gamma stimulation mitigates the effects of demyelination induced by cuprizone in male mice. Nature Communications, 2024. 15(1): p. 6744.
39. Zirngibl, M., et al., Oligodendrocyte death and myelin loss in the cuprizone model: an updated overview of the intrinsic and extrinsic causes of cuprizone demyelination. Molecular neurodegeneration, 2022. 17(1): p. 34.
40. Baltan, S., et al., Neuronal hibernation following hippocampal demyelination. Acta neuropathologica communications, 2021. 9(1): p. 34.
41. Serneels, P.-J., et al., Oligodendroglial heterogeneity in health, disease, and recovery: deeper insights into myelin dynamics. Neural Regeneration Research, 2025. 20(11): p. 3179-3192.
42. Das, A., et al., Reversible Loss of Hippocampal Function in a Mouse Model of Demyelination/Remyelination. Frontiers in Cellular Neuroscience, 2020. 13(588).
43. Jhelum, P., et al., Ferroptosis mediates cuprizone-induced loss of oligodendrocytes and demyelination. Journal of Neuroscience, 2020. 40(48): p. 9327-9341.
44. Roufagalas, I., et al., Novel cell-based analysis reveals region-dependent changes in microglial dynamics in grey matter in a cuprizone model of demyelination. Neurobiology of Disease, 2021. 157: p. 105449.
45. Ramaglia, V., et al., Complement-associated loss of CA2 inhibitory synapses in the demyelinated hippocampus impairs memory. Acta neuropathologica communications, 2021. 142(4): p. 643-667.
46. Zhan, J., et al., The cuprizone model: dos and do nots. Cells, 2020. 9(4): p. 843.
47. Gudi, V., et al., Glial response during cuprizone-induced de- and remyelination in the CNS: lessons learned. Frontiers in Cellular Neuroscience, 2014. 8.
48. Zhang, H., et al., Hippocampal neurogenesis and neural circuit formation in a cuprizone-induced multiple sclerosis mouse model. Journal of Neuroscience, 2020. 40(2): p. 447-458.
49. Schröder, L.J., et al., Dynamics of reactive astrocytes fosters tissue regeneration after cuprizone-induced demyelination. Glia, 2023. 71(11): p. 2573-2590.
50. Luo, F., et al., Cuprizone-induced demyelination under physiological and post-stroke condition leads to decreased neurogenesis response in adult mouse brain. Experimental neurology, 2020. 326: p. 113168.
51. Molinari, Y.A., et al., The effects of Cuprizone on murine subventricular zone-derived neural stem cells and progenitor cells grown as neurospheres. Molecular Neurobiology, 2023. 60(3): p. 1195-1213.
52. Hahn, K.R., et al., Cu, Zn-superoxide dismutase has minimal effects against cuprizone-induced demyelination, microglial activation, and neurogenesis defects in the C57BL/6 mouse hippocampus.

Neurochemical Research, 2023. 48(7): p. 2138-2147.
53. Hahn, K.R., et al., Therapeutic Options of Crystallin Mu and Protein Disulfide Isomerase A3 for Cuprizone-Induced Demyelination in Mouse Hippocampus. Neurochemical Research, 2024. 49(11): p. 3078-3093.
54. Escartin, C., et al., Reactive astrocyte nomenclature, definitions, and future directions. Nature neuroscience, 2021. 24(3): p. 312-325.
55. Marangon, D., et al., Oligodendrocyte progenitors in glial scar: a bet on remyelination. Cells, 2024. 13(12): p. 1024.
56. Bu, J., et al., Paroxetine ameliorates corticosterone-induced myelin damage by promoting the proliferation and differentiation of oligodendrocyte precursor cells. Neuroscience, 2025. 573: p. 344-354.
57. Rosen, D.A., et al., Modulation of the sigma-1 receptor–IRE1 pathway is beneficial in preclinical models of inflammation and sepsis. Science translational medicine, 2019. 11(478).
58. Zou, Y., et al., Fluvoxamine inhibits Th1 and Th17 polarization and function by repressing glycolysis to attenuate autoimmune progression in type 1 diabetes. Molecular Medicine, 2024. 30(1): p. 23.
59. Hashimoto, K., Viewpoints Sigma-1 receptor agonist fluvoxamine for multiple sclerosis. Brain, Behavior, Immunity-Health, 2024. 37: p. 100752.
60. Eskandari, K., et al., Repurposing Sigma-1 Receptor-Targeting Drugs for Therapeutic Advances in Neurodegenerative Disorders. Pharmaceuticals, 2025. 18(5): p. 700.
61. Shi, M., et al., Fluvoxamine confers neuroprotection via inhibiting infiltration of peripheral leukocytes and M1 polarization of microglia/macrophages in a mouse model of traumatic brain injury. Journal of neurotrauma, 2022. 39(17-18): p. 1240-1261.
62. Tepebaşı, M.Y., et al., Potential Ameliorating Effects of Fluvoxamine in a Rat Model of Endotoxin-Induced Neuroinflammation: Molecular Aspects Through SIRT-1/GPX-4 and HMGB-1 Signaling. Molecular Neurobiology, 2025. 62: p. 7892–7902.
63. Elbeltagy, M., et al., Fluvoxamine Ameliorates the Damage to the Neuro-Behavioral Status of Rats Caused by the Administration of Valproic Acid by Preventing Cognitive Memory Deficits and Decreased Hippocampal Cellular Proliferation. Cureus, 2024. 16(4): p. 1-14.

